Brooks, B.E., and Beckermann, C., "Prediction of Heat Treatment Distortion of Cast Steel C-Rings," in Proceedings of the 61st SFSA Technical and Operating Conference, Paper No. 4.5, Steel Founders' Society of America, Chicago, IL, 2007.

PREDICTION OF HEAT TREATMENT DISTORTION OF CAST STEEL C-RINGS

Brandon Elliott Brooks[1] and Christoph Beckermann[2]

[1]Graduate Research Assistant and [2]Professor, Department of Mechanical and Industrial Engineering, The University of Iowa, Iowa City, Iowa 52242, USA

Abstract

Navy C-Ring test parts were made of AISI 1022, 4320, 8625, and CF8M steels and heat treated in a designed experiment to evaluate the commercial heat treatment distortion simulation software DANTE. The parts were machined and then measured with a CMM for original dimensions. The parts were then heated and subsequently quenched in two different immersion orientations in agitated water. Temperature measurements were taken from the austenitic stainless steel parts to obtain heat transfer coefficients for the simulations. The part dimensions were re-measured and compared to pre-heat treatment values. The CF8M experiments show that the gap in the C-Ring closes due to thermal stresses. The cast carbon and low-alloy steel C-Rings resist the closure somewhat, though general trends toward closure are still apparent. This is in contrast to results shown in previous literature. The dimensional measurements for the different immersion directions and different alloys are compared and discussed. While the DANTE simulations are able to capture the general distortion trends seen in the experiments, they are not in complete agreement with the experimental results obtained here. Recommendations are made for future work.

Introduction

Optimal efficiency in the production of steel castings is often hindered by distortions that occur during heat treatment. These distortions can arise regardless of whether the parts are severely quenched, or normalized and annealed. Distortions can take place in castings of all sizes and shapes. Heat treatment distortion can be costly [1, 2]. The cost is normally incurred through extensive rework or redesign, recasting, or through additional machining steps. Predicting heat treatment distortion is difficult, and correcting distortion problems is often a lengthy trial-and-error process.

There has been extensive interest in the prediction of heat treatment distortion via computer simulation for about the last 40 years. Original simulations designed to predict distortions seen in heat treated parts encompassed a single physical phenomenon, such as thermally induced stresses, in two dimensions. Simulations gradually grew in complexity to three-dimensional finite element analyses with multiple physical phenomena coupled together [1-29]. The parts studied to validate software packages are normally forged or machined from stock, and are small and carburized. As of the writing of this paper, no study has been identified in the literature that evaluates commercial heat treatment software programs specifically for steel castings.

Many of the simulation results presented in the literature are shown to be in good agreement with experiments in terms of residual stress, carbon levels (for diffusion simulations), phases present,

and hardness. Most studies also report good agreement in terms of part distortion, but do so mostly qualitatively. Often, the methodology for measuring the parts is only briefly mentioned. Finally, there is still reason to believe that some of the predictions of distortion are completely erroneous. Some experiments show distortions that are unpredicted and unexplainable. Not only that, some research indicates that independent of the modeling methods employed, certain unknown factors can and will affect distortion measured in heat treated parts.

Research is still needed to validate commercial heat treatment software for cast steel parts, by employing a variety of heat treatment schedules and steel alloys. The objective of the current research is to test the suitability of the commercial simulation software DANTE[1] for predicting heat treatment distortion of steel castings. Work on this project was begun by Hardin and Beckermann in 2005 [4], and preliminary results were presented at the 2005 SFSA T&O conference that illustrate the simulation capabilities of the DANTE software [4].

Experiments were designed to encompass many of the lacking elements of the current literature. Multiple grades of carbon and low-alloy steel (AISI 1022, 4320 and 8625) were cast and machined into C-Ring test parts [30-32]. The C-Rings were heat treated, using both vertical (for symmetric distortions) and side (for asymmetrical distortions) immersion directions during water quenching. Dimensional measurements were performed in an accurate and repeatable manner. Austenitic CF8M steel C-Rings were cast and heat treated using the same schedule as for the carbon and low-alloy steels, in order to aid in the evaluation of the experimental procedures and the simulation software. Note that there are no phase transformations occurring during heat treatment of CF8M steel. Temperature measurements were taken during the heat treatment of the CF8M C-Rings, and a trial-and-error method was used to back out heat transfer coefficients for use in the DANTE simulations. The heat treatment was simulated for each carbon and low-alloy steel and for each immersion direction. Comparison between measured and predicted results was then used as a means of evaluating the suitability of the DANTE software for steel castings.

Background in Modeling Heat Treatment with DANTE

There have been numerous attempts at mathematically modeling the heat treatment of steel. Successful attempts at predicting heat treatment distortion always include three different analysis steps: phase transformation analysis, temperature analysis, and stress analysis. The analyses are performed with the aid of commercial finite element or computer aided engineering software packages. While the DANTE (Distortion ANalysis for Thermal Engineering) software program is being investigated in this paper, older programs such as HEARTS, and newer programs such as DEFORM-HT[2] have also been studied [3, 4, 9, 17, 26].

DANTE is the result of a multi-million dollar investment of corporate, scholastic, and federal funds. DANTE is a series of subroutines that operate under the ABAQUS CAE[3] finite element software that simulates the phase (or metallurgical) transformations, thermal evolution and the resulting mechanical response during heat treatment [1, 5, 6, 22-25, 29]. DANTE can also be used for the simulation of hardening processes through the use of a carbon-diffusion model.

[1] http://www.deformationcontrol.com/
[2] http://www.deform.com/ht_brochure.pdf
[3] http://www.simulia.com/

The mathematics of the phase/temperature/stress analyses is highly complex and is explained fully in Refs. [1-28]. A good visualization of what the modeling entails is shown Fig. 1, including how and where user inputs are entered [6, 24].

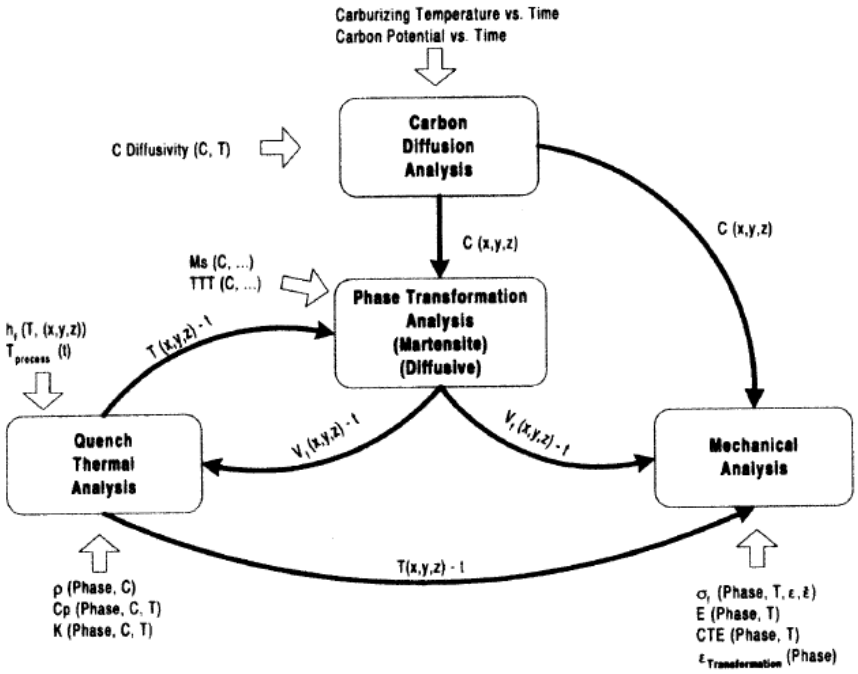

Figure 1. Diagram showing the user inputs and the 'black box' operations of the mathematical model used in DANTE

In simulating heat treatment, DANTE solves for the phase transformations and the thermal evolution in a coupled manner. The phase transformations are calculated based on isothermal transformation diagrams, continuous cooling diagrams, as well as martensite transformation information. The prediction of the temperature variations depends primarily on the accurate knowledge of the heat transfer coefficients on the surfaces of the modeled part and of the temperature dependent thermo-physical properties. However, the thermo-physical properties vary with phase and phase fraction. Therefore, the phase transformations and temperature evolution need to be solved in a coupled manner. DANTE does this in one analysis step and stores all of the calculated temperatures, volume changes and phase fractions as a function of time and position in a result file. This calculated data is then used as input in the stress analysis. A so-called 'internal state variable,' discussed below, is continually updated so that the simulation is completed is a semi-coupled fashion.

The mechanical analysis in DANTE uses the Bammann-Chiesa-Johnson (BCJ) material model, which employs an internal state variable based on 27 different parameters to describe the state of the material. The mechanical properties were created from experiments at various temperatures, strains and strain rates [1, 5, 6, 22-25]. Similar to the HEARTS model developed in the 80s and 90s [9, 16, 17, 26], the mechanical model also includes the transformation induced plasticity (TRIP) inherent in phase changes. Neglecting these TRIP effects was shown to predict deformations poorly, so the added complexity is justified [9, 24, 28]. For mixed phases (such as half ferrite and half Pearlite) mixture rules are used. The data for the mechanical model was obtained by rigorously controlled mechanical testing with varied carbon contents. As of this writing, the DANTE data base contains date for approximately twenty low-alloy steel families and a few high hardness alloys.

The phase transformation data was obtained from dilatometry experiments at various carbon contents. Tests were conducted at 0.20%, 0.40% and 0.60% carbon by weight, so that data for any other carbon content can be interpolated.

The elastic properties and the thermo-physical properties in DANTE were taken from the literature. All of the phase change data and physical properties were then conformed to the BCJ model. References [1] and [6] give a detailed account of these methods from the researchers directly involved in the creation of DANTE.

The primary outputs of the mechanical analysis are the residual stresses in and the final dimensions and distortions of the heat treated part. DANTE also predicts the final phase fractions, including ferrite, pearlite, upper and lower bainite, martensite and tempered martensite. Vickers hardness is also calculated. The outputs are visualized in ABAQUS CAE.

Experiments

The part chosen for the present experiments is a modified Navy C-Ring, a version of which is shown in Fig. 2. The geometry was changed to aid in casting. C-Rings were cast of CF8M, 1022, 4320, and 8625 steel. The cast C-Rings were then machined to remove rough surfaces and to enable the dimensional measurements. The C-Rings were measured with a coordinate measurement machine (CMM). They were then coated in stop-off paint, embedded with thermocouples, and heat treated in a foundry laboratory. The parts were then re-measured, and the amount heat treatment distortion was quantified. This section details some aspects of the experiments.

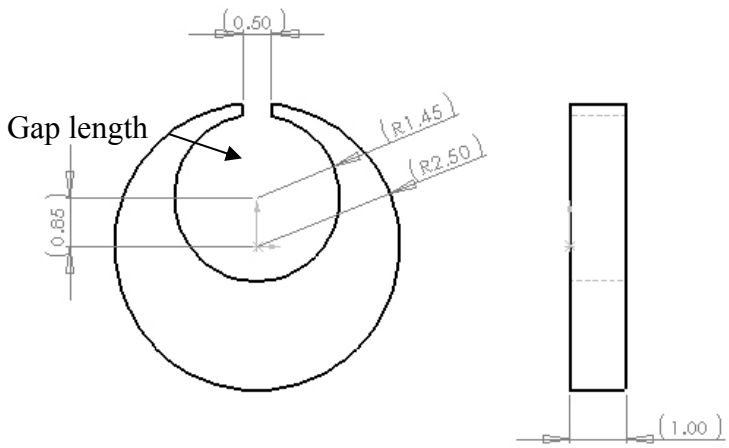

Figure 2. Original design of the Navy C-Ring

The C-Ring Test Part. C-Rings have historically been used to test the severity of different quenching materials [30-32]. During the tests, the C-Rings have traditionally been heated to above the Ac_3 temperature, and quenched in still or agitated water, oil, or cooled in still and forced air [30-32]. Because of the unique shape of the part, namely the gap and the offset circles that form tapered prongs, the cooling rates during quenching vary throughout the part. These non-uniformities cause phases to transform at different locations in the part at different times. They also result in thermal stresses and plastic deformation. The amount of distortion is primarily controlled by carbon content, other alloying constituents, and quenching procedures.

Traditionally, the distortion of interest for the C-Ring is the distance between the prong tips, the so called 'gap length.' For austenitic steels, the gap tends to close during water quench processes because of thermal stresses [32]. That is in contrast to the gap opening seen in nearly every other type of steel that undergoes some amount of phase transformation [30-31].

Casting the C-Rings. The dimensions of the C-Ring that were used in the design of the pattern are provided in Fig. 2. The pattern was made at a foundry. Draft angles and all other pattern considerations were made by the pattern maker with the goal of achieving the dimensions seen in Fig. 2. The original goal was to cast the C-Rings as close as possible to the geometry shown in Fig. 2. The initial attempts included casting of the C-Ring with a core in the center of the inner diameter and a spacer core at the gap. However, casting the approximately 0.2 inches thin C-Ring prong tips proved to be unsuccessful.

Thus, the pattern was changed to the closed-gap ring configuration shown in Fig. 3. The tapered section was made nominally thicker for the closed ring to aid in producing sound castings. The C-Ring castings were produced at two different foundries.

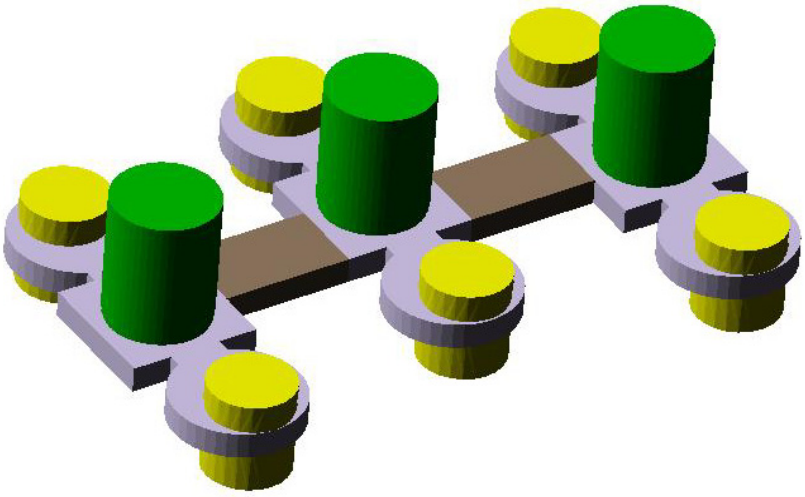

Figure 3. Final casting configuration, shown in MAGMASoft[4]

Machining the C-Rings. The as-cast rings were machined to the unique final C-Ring geometry shown in Fig. 4 (a technical drawing is provided in Appendix A). Several features were added to the original C-Ring design to aide in measurement, instrumentation, and execution of the experiments, notably, a small groove, a flat base, two support holes, and a thermocouple well.

When measuring distortions induced by heat treatment, the goal is to obtain the relative differences in the dimensions from before to after heat treatment. In other words, deformations and distortions are expressed relative to the initial shape of a part. However, the dimensional measurements were made on a coordinate measurement machine whose output is three dimensional distance from an arbitrary reference point, on an arbitrarily chosen datum. Therefore, it is not possible to measure the relative differences in the dimensions accurately unless the reference point and the datum planes are defined and marked on the part itself. The shallow groove and the flat base were added so that a reference point and datum planes could be found in a repeatable manner.

As shown in Fig. 4, the reference point is located in between the vertical sides of the groove, on the corner of the grove and the flat base. In terms of the datum planes, the y-z plane is formed by the flat base, the y-x plane is defined by the vertical sides of the groove, and the x-z plane is defined by the base of the groove. The centerline of the part and the flat base are not expected to distort significantly during heat treatment. The result of adding the groove and the flat base to the C-Ring is that the C-Ring can be placed in any location and orientation on the CMM platform, and that the dimensional measurements before and after heat treatment can be directly compared.

[4] http://www.magmasoft.com/

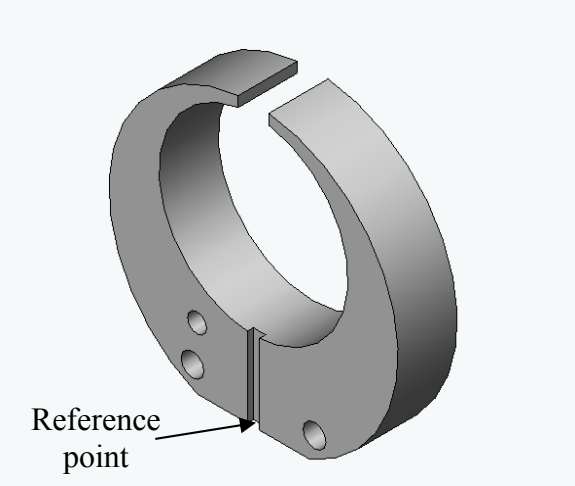

Figure 4. Image of a solid model of the final machined C-Ring

The two support holes seen in Fig. 4, symmetric about the y-x plane, were added to enable gripping of the part during immersion into the quench tank. Also shown in Fig. 4 is a thermocouple hole above the left support hole. The gripping of the parts during quench, the immersion rack, and the thermocouple design are discussed in later subsections.

Dimensional Measurements. Dimensional measurements were performed using a Sharpe and Brown[5] CMM with a 1 mm diameter stylus tip on an 80 mm long stylus arm. The C-Rings were laid flat on the surface of a standard steel grid with the groove facing up. The C-Rings were not secured with a vice, or by other means. It has been found that even a small external compressive force on the C-Ring can lead to measurement errors [33].

The measurement procedure was to first determine the three orthogonal datum planes and find the reference point (located at the intersection of the three datum planes). The stylus of the CMM was then moved by a hand-held controller, and a two dimensional outline of the part was found by touching the C-Ring surface at approximately mid-thickness in sequential locations around the part. A program was written for the CMM machine so that every measurement, except for the initial location of the reference point, was automated. The locations of the measured points were then plotted on a Microsoft Excel®[6] graph. An example is shown in Fig. 5, where the unit is mm. By measuring the same part three different times, it was determined that the dimensional measurements were repeatable to within 0.011 mm.

[5] http://www.brownandsharpe.com/
[6] http://office.microsoft.com/en-us/excel/default.aspx

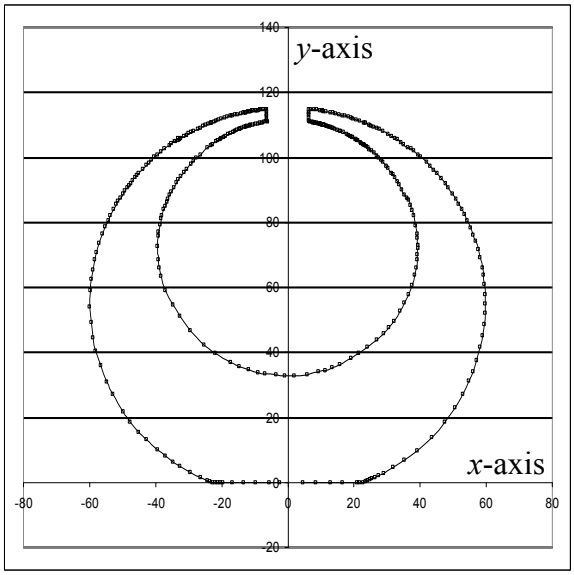

Figure 5. Example of dimensional measurements made on the C-Ring (in mm)

Thermocouples. A single type-K thermocouple was placed in several of the C-Rings. The thermocouples were obtained from Omega[7]. The thermocouples were covered with glass cloth, which can sustain temperatures up to at least 2200ºF without failure. The thermocouple was placed inside a bent steel tube. The steel tube was press fit into the thermocouple hole in the C-Ring. Steel tubes were used to ensure that the thermocouples did not contact the water in the quench tank. Although the thermocouple wires were covered in temperature resistant cloth, the cloth was not waterproof. The tubes, which were thin-walled and 12 inches long, were also ordered from Omega. The thermocouples were connected to Cu-Cu extension wires that were 18 feet long. The thermocouples were connected to a computer data acquisition system running the DasyLab[8] program. The sampling rate was at set at 10 Hz.

Quench Rack. Controlling immersion is vital to the repeatability of the experiments. A quench rack that ensured control during immersion was designed and is shown in Fig. 6. The quench rack allowed for the C-Rings to be quenched with either the prong tips both facing downward, or with one side immersed first. The two different gripping styles are illustrated in Fig. 7.

[7] http://www.omega.com/
[8] http://www.dasylab.com/

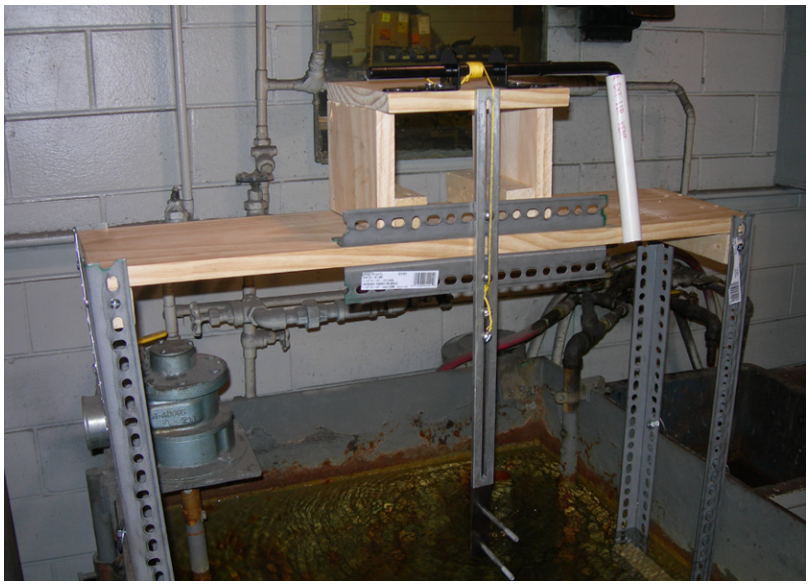

Figure 6. Picture of the quench rack used in the experiments

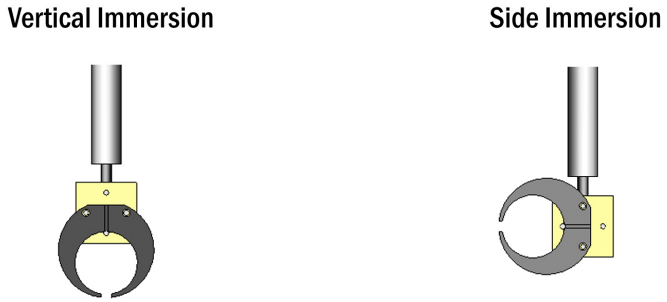

Figure 7. Different directions of immersion used in the present study

The quench rack stand was designed specifically for the quench tank seen in the lower part of Fig. 6. The tank is a 30 inch cube with a seven inch water board. The angle irons shown are used as support legs and are bolted to the side of the tank. The black rod, with yellow string wrapped around it, is a reel that was used to lower the parts into the water. The yellow string was attached to a steel dip stick, which is guided by an aluminum track and two angle irons. The cross beam and box were made from pine wood. The piece of PVC seen in Fig. 6 was used as a stop for the reel. The rack is shown for the side immersion process.

The parts were taken from the oven in a pair of tongs, moved to the rack and placed on the holding pins, which were made of galvanized steel bolts. The parts were then lowered into the water. The water in the quench tank was always agitated while the parts were immersed. The air-powered impellor is 6.5 inches in diameter and was located at the bottom of the tank in a corner. The water was flowing at 9 to 10 feet per second. The quench tank was qualified by the foundry in which the experiments were performed.

Experimental Procedure. This section outlines the procedure that each of the cast C-ring test parts underwent.

1. Casting – the parts were cast in a 'six-on' configuration. The steels were poured under standard foundry conditions. The CF8M castings were produced at one foundry, and the other alloys, 1022, 4320 and 8625, were cast at a second foundry.

2. Cleaning the castings – the gates and risers were removed from the rough castings with arc-torches.

3. Machining – the residual base material left over from the cleaning step was cut from the parts. Then, the closed ring parts were machined flat on the top and bottom. The center of the inner ring was then located on a CNC vertical milling machine. The outer ring was also located, and the two support holes were drilled. The following machining steps included milling of the flat base, the inner and outer diameters, the gap opening and the groove. Finally, if needed, the thermocouple well was bored. The machining procedure was the same for all parts.

   The parts were then de-burred by hand with a combination of metal files. The residual metal burrs that adhered to the C-Rings were removed by demagnetizing the C-Rings. Each part was taken through a magnetic field twice, once with each side facing the magnetic field. They were then taken and washed in solvent to remove any cutting grease or residual oils on the surface. The solvent was applied with a soft bristled brush with ample amounts of flow to completely rinse the parts free of oils and metal burrs. The parts were then blown dry with a standard metal-shop compressed air nozzle.

4. Measurement #1 – The C-Rings were measured on a Brown and Sharpe coordinate measurement machine (CMM) in the metrology lab at Iowa State University. The parts were placed flat onto a standard measurement block with the measurement groove side up. The parts were consistently aligned with the use of guide rails. The reference point was found by using a hand held controller to find the bottom of the groove which was defined as a plane by touching it three times at distant locations. The left hand side of the groove was touched twice by the stylus and called a straight line in the PCDMIS controlled computer, as was the flat machined base. The two intersecting lines and plane formed the axis on the part and were described as orthogonal in the CMM. A program was written that took more than 370 points on the side and top of the part.

5. Painting with Stop-Off Paint – the parts were then coated in Condursal[9] Stop-Off paint. The pieces were painted on one side with a soft bristle brush, left to dry for several hours, and then flipped and coated on the other side.

6. Heat Treatment – All of the parts were put into a small box oven in small batches of between two and 15. The oven was set to compensate for the known offset. The parts were left to heat for at least 30 minutes at 881ºC.

   The door was opened and each part was taken in a pair of hand held metal tongs and gripped on the right hand side of the C-Ring. The C-rings were moved according to one of the schedules below:

   - Water Quench, Vertical Immersion – The parts were placed on the immersion stand so that both prong tips of the C-Ring were the first parts to touch the water. The transfer time was recorded. The part was then immersed quickly into the well agitated water. They were left there for five minutes.

   - Water Quench, Side Immersion – The part was placed on the immersion stand so that the outer diameter on the left side of the C-Ring would touch the water first, followed by the left prong tip, and so on. The transfer time was recorded. The part was then immersed quickly into the well agitated water and held for five minutes.

7. Washing – the parts were washed in agitated warm water, about 40ºC, to remove the stop-off paint.

8. Measurement #2 – the parts were then re-measured in the same fashion as the pre-heat treat measurements, and using the same program as outlined in step #4.

Temperature Measurements and Determination of Heat Transfer Coefficients

Temperature measurements are crucial in evaluating a heat treatment process, as well as for performing reliable simulations. The temperature measurements are also used in the present study to determine the temperature dependant heat transfer coefficients during the experiments. Note that all C-Rings were subjected to the same oven, ambient air, and quench tank environments.

Background in Boiling. When a water quench is used to cool a part, there are three distinct modes of heat transfer that are important (sometimes, two additional transition modes are also defined) [34]. A diagram of the three different modes is shown in Fig. 8, along with the two transition modes. The three main modes are film boiling, nucleate boiling, and convective cooling. The figure, taken from Ref. [37], shows a representative temperature vs. time curve taken from the center of a part during quenching.

[9] http://www.duffycompany.com/Condursal_0090.htm

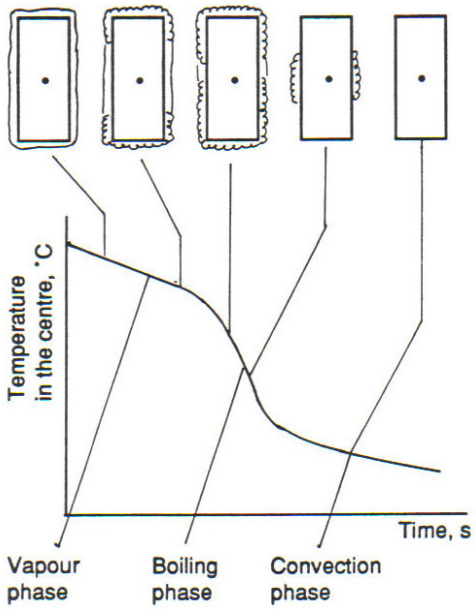

Figure 8. Three modes of boiling on a temperature vs. time chart during a water quench [37]

In the film boiling mode, the surface of the steel is so hot that no liquid touches the surface and a stable vapor film is formed. The vapor film acts as an insulator, which results in a relatively low heat transfer coefficient. When a part is quenched, the internal temperature drops noticeably when the film boiling phase begins and an inflection point can be observed on the cooling curve. When the surface temperature drops to a point where liquid comes into contact with some parts of the surface, the transition to nucleate boiling region can be identified by another inflection point on the cooling curve. The nucleate boiling mode is where most of the heat transfer takes place and where the largest temperature drop occurs. The transition to the third mode (convective cooling) occurs smoothly with no sharp inflection point. The convective cooling mode features the lowest heat transfer coefficient.

Determination of Heat Transfer Coefficients. Temperature versus time data was collected from three CF8M parts undergoing heat treatment. They are plotted in Fig. 9. The cooling curves were superimposed by adding or subtracting different amounts of time to the original data to align the curves at the various transition points between the heat transfer modes. It can be seen that the temperature measurements are almost identical for the three experiments. Also plotted in Fig. 9 are cooling rates, which were obtained by taking the time derivative of the measured temperature variations. Again, good agreement can be observed among the three experiments.

Simulations were performed to determine the heat transfer coefficients in a trial-and-error methodology. The part geometry was modeled in SolidWorks[10] and imported into ABAQUS CAE. An input file was written that included a heat up step, an air transfer step and a quench

[10] http://www.solidworks.com/

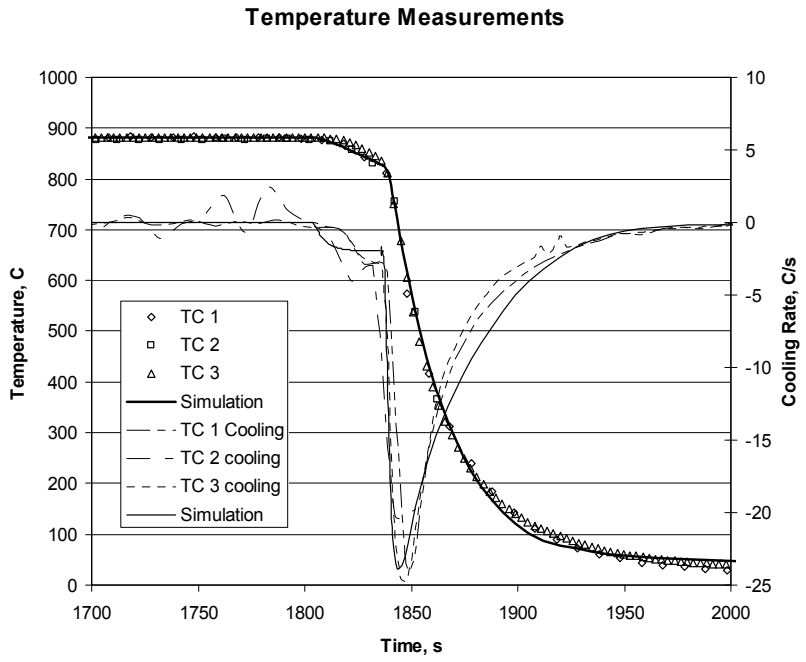

Figure 9. Temperatures and cooling rates measured as a function of time in three experiments, and comparison with predicted temperatures and cooling rates from the simulation

step. The immersion was not simulated. DANTE does not have a material data base for CF8M or similar stainless steel grades. Therefore, the thermal analysis was done solely on the ABAQUS CAE platform. The thermo-physical properties for CF8M were created using JMATPro[11], a commercial software program that predicts properties of steels (and other metal alloys) of a given composition. Based on thermocouple measurements made during the casting of the CF8M C-Rings and comparisons with corresponding casting simulations (not reported here), the thermo-physical properties obtained from JMATPro are believed to be accurate throughout the temperature range of interest.

Standard temperature dependant still air, furnace and water quench heat transfer coefficients from DANTE were used as initial guesses in the simulations. The results of the initial simulations were compared to the measured cooling curves and cooling rates. Adjustments were made to the heat transfer coefficients until the simulated and measured cooling curves and cooling rates agreed closely.

The heat transfer coefficients determined in the above manner are shown graphically as a function of temperature in Fig. 10. For the quench, the heat transfer coefficient follows the expected modes of heat transfer associated with boiling. Specifically the graph shows high heat transfer coefficients during nucleate boiling and lower heat transfer coefficients during film boiling and convective cooling.

[11] http://www.thermotech.co.uk/

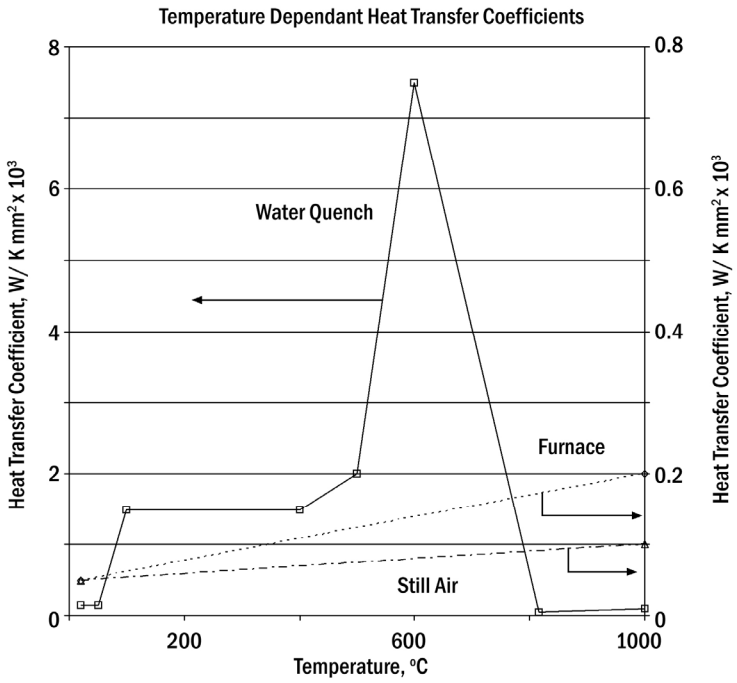

Figure 10. Temperature dependant heat transfer coefficients used in the simulations

Using the heat transfer coefficients plotted in Fig. 10 in the simulation produces excellent agreement between measured and predicted temperatures and cooling rates as a function of time, as shown in Fig. 9. The heat transfer coefficients in Fig. 10 do not necessarily match other published data because the heat transfer conditions, e.g., the water agitation in the quench tank, are different in each heat treatment setup.

Analysis of Dimensional Data and Experimental Results

Analysis of Dimensional Data. The major difficulty when measuring distortion or deformation with a CMM is that changes in material location are not tracked directly. Instead, only outlines of the parts are recorded. When comparing before and after heat treatment measurements of the same part, the displacement of a given material point is therefore not immediately known.

Because of this difficulty, lines were fit through data points that formed the outlines of the C-Ring prong tips. The lines were used to locate the corners of the prong tips, which represent material points. By comparing the locations of the corners of the prong tips from before to after heat treatment, corner displacement vectors were obtained.

The points taken with the CMM near a prong tip were fit with a straight line and two splines. An example of this analysis is shown in Fig 11. It was found that improved accuracy could be obtained by rotating the data by 90 degrees about the z-axis. This was done with a rotation matrix in Excel®. The flat end of a tip was approximated by a straight line, and the outer and

inner diameters formed arcs that were approximated by second order polynomial splines. The intersections of the flat end line and the splines were used to locate the two corner points. The deformation is then quantified by tracking the movement of each corner from before to after heat treatment. Deformation vectors were calculated by subtracting the x-y locations of the corners from before to after heat treatment to obtain the magnitude of the deformation as well as the direction in which the corners were displaced.

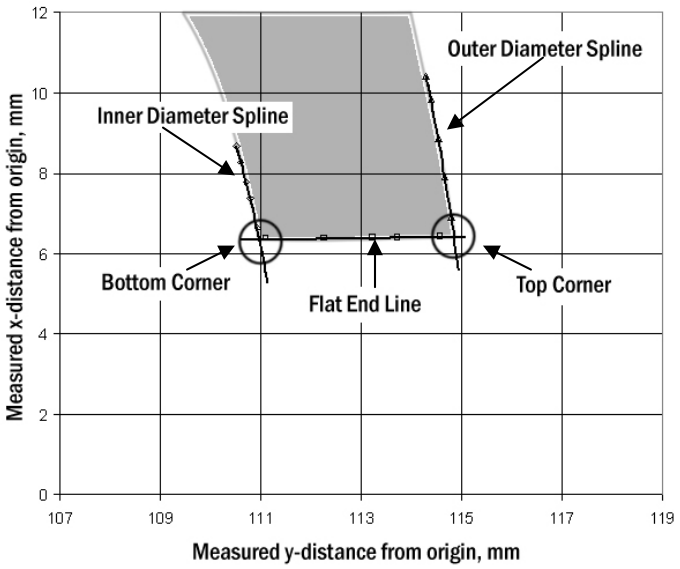

Figure 11. Method used to locate the corners of the prong tips

A schematic of the present gap analysis is shown in Fig. 12. The average gap length is defined as the mean distance between the two corners of the "left" prong tip and the opposing two corners of the "right" prong tip of a C-Ring. In other words, it is the distance between the two mid-points of the straight end lines that extend between the "bottom" and "top" corners of each prong tip. By subtracting the average gap lengths measured before and after heat treatment, the gap opening (or closing) is obtained. The gap opening represents the most important figure of merit used in the present heat treatment distortion analysis. The direction of the movement of each prong tip in the *x*-*y* plane was also recorded. The *x*-direction displacement (from before to after heat treatment) of a prong tip represents the "lateral" movement of the mid-point of the straight end line between the two corners of the tip, while the *y*-direction displacement is the "vertical" movement of the mid-point. Here, the hyphenated terms refer to the orientation of the C-Ring shown in Fig. 5.

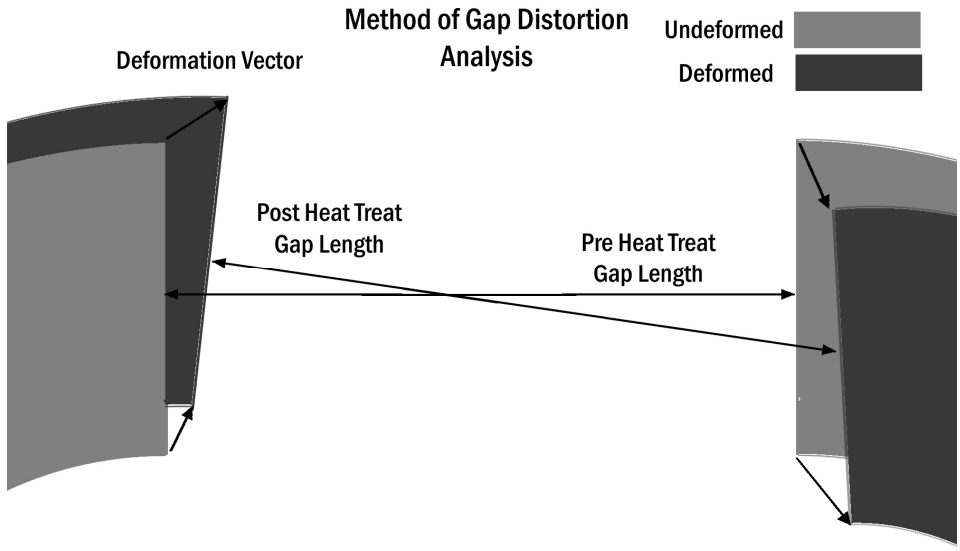

Figure 12. Schematic of the present gap distortion analysis

Introduction to Experimental Results. In the following subsections, detailed results are only presented for the CF8M side immersion experiments. The results for all other experiments are only presented in summary form, and the reader is referred to Ref. [47] for a complete account of the measurements. A total of eight sets of experiments were conducted: CF8M side immersion (5 C-Rings); CF8M vertical immersion (4 C-Rings); 1022 side immersion (5 C-Rings); 1022 vertical immersion (5 C-Rings); 4320 side immersion (5 C-Rings); 4320 vertical immersion (5 C-Rings); 8625 side immersion (5 C-Rings); and 8625 vertical immersion (5 C-Rings). Thus, each type of experiment, except one, is repeated five times. Average deformation vectors and gap closings are presented for each of the eight sets of experiments and compared.

CF8M Side Immersion Experimental Results. Figure 13 shows measured outlines of the prong tips for each of the five CF8M water quenched side immersion test parts without any magnification of the distortion. The numerical values for the dimensional changes experienced by the C-Ring prong tips are provided for each experiment in Table 1. A bar graph of the changes in the gap length is presented in Fig. 14. Results are presented for each C-Ring, because it is important to see the differences from experiment to experiment. In general, the gap formed by the prong tips closes in all five experiments. Even though the C-Rings were immersed in the side direction, most of the prong tips translate towards each other in a fairly symmetric manner. All of the tips also translate in the negative y-direction (i.e. towards the center of the C-Ring). The average change in gap length is -0.70 mm with a standard deviation of 0.16 mm. The left side, the side immersed first, accounts for -0.30 mm of the gap change and the right side accounts for -0.41 mm of the gap closure. Overall, the results of the five experiments are quite consistent. This suggests that the experimental procedure and method of analysis are generally accurate and repeatable.

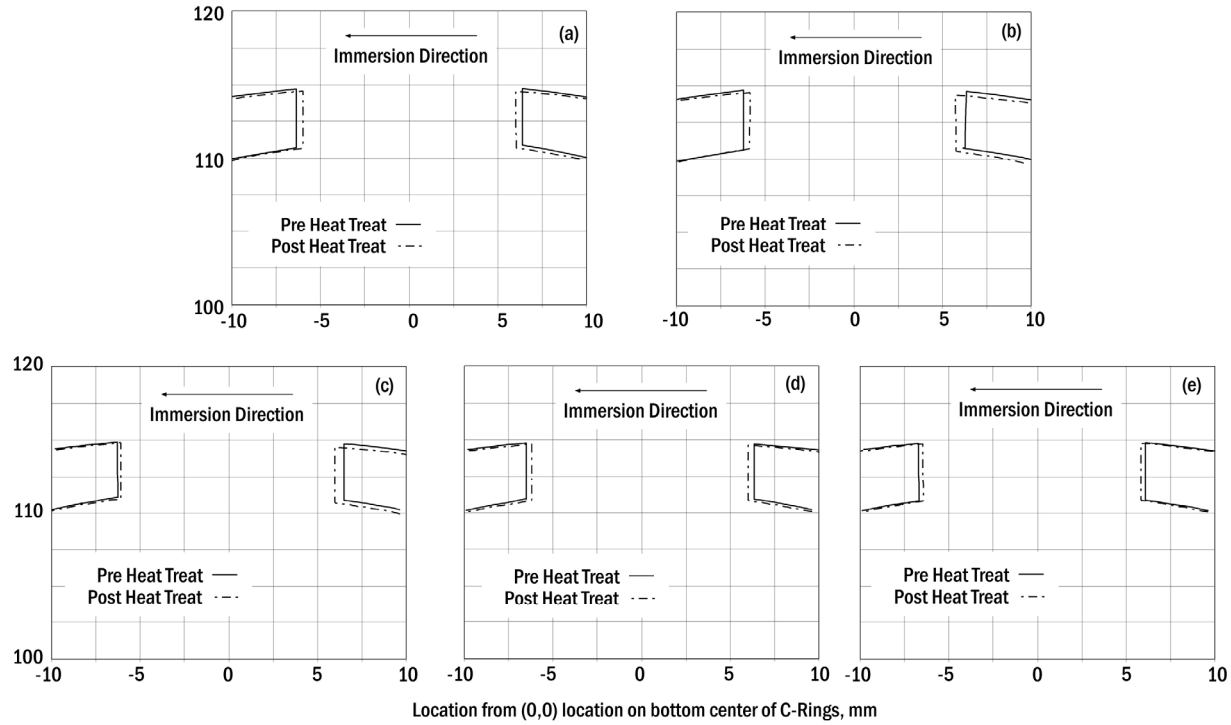

Figure 13. Plots of the before and after heat treatment prong tip outlines for the CF8M water quench side immersion experiments

Table 1. Results for the CF8M water quench side immersion experiments

	Left Side, mm		*Right Side, mm*		*Gap*
Test Part	**X-direction**	**Y-direction**	**X-direction**	**Y-direction**	**Opening, mm**
CF8M a	-0.37	-0.15	-0.36	-0.20	**-0.74**
CF8M b	-0.36	-0.13	-0.57	-0.23	**-0.93**
CF8M c	-0.19	-0.08	-0.53	-0.18	**-0.72**
CF8M d	-0.31	-0.07	-0.35	-0.08	**-0.65**
CF8M e	-0.25	-0.02	-0.25	-0.03	**-0.50**
Average	-0.30	-0.09	-0.41	-0.14	**-0.70**
Standard Dev	0.07	0.05	0.13	0.09	**0.16**

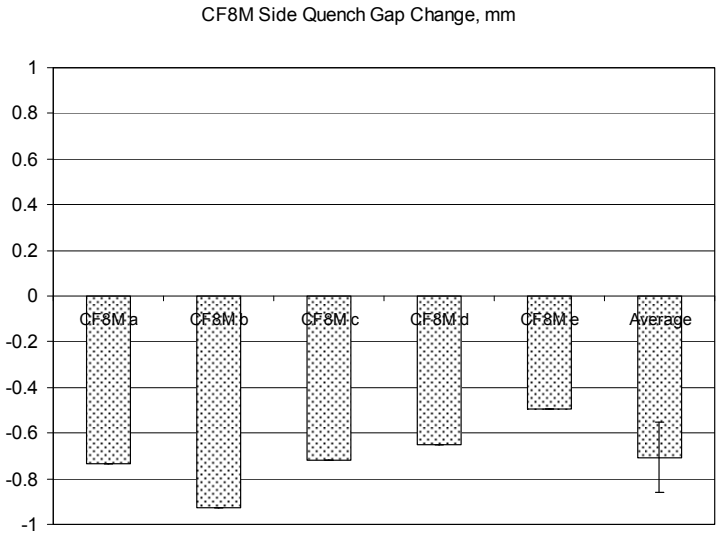

Figure 14. Bar graph of the gap changes in the CF8M water quench side immersion experiments

Comparison of CF8M Vertical and Side Immersion Experimental Results. Figure 15 shows a comparison of the CF8M vertical and side immersion results. The three types of prong tip outlines shown in this figure represent averages for all nine CF8M pre heat treat, five CF8M side immersion post heat treat and four CF8M vertical immersion post heat treat C-Rings. In order to

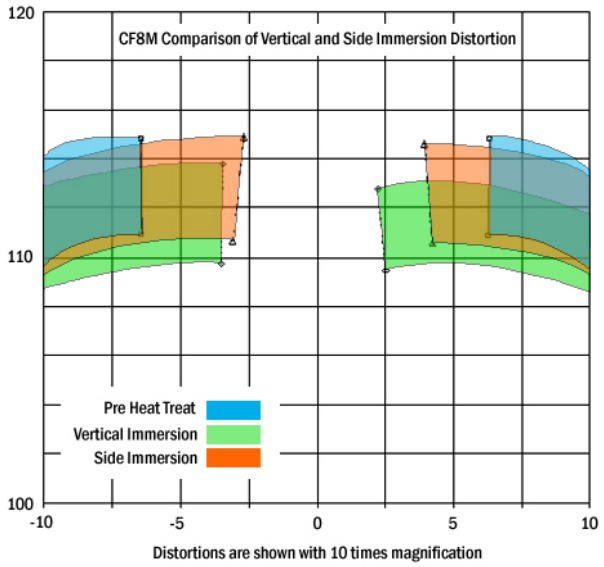

Figure 15. Comparison of the CF8M vertical and side immersion average prong tip outlines (10 times amplification of the deformations)

better visualize the deformations, they were amplified by multiplying the magnitude of the deformation vectors for each corner by a factor of ten.

The comparison of the CF8M experiments shown in Fig. 15 indicates that there is a difference in the distortions between the vertical and side immersion experiments. The gap in the side immersion experiments tends to close more (-0.71 mm on average) than in the vertical immersion experiments (-0.55 mm on average). Furthermore, the gap change for the vertical immersion direction appears to be more asymmetric than the gap change for the side immersion experiments. However, this asymmetry is caused by a single outlying case in the vertical immersion experiments [47]. These results do not immediately lend themselves to an easy explanation of what is physically occurring.

Summary of Results for All Experiments. A summary of the average gap openings for all eight sets of experiments performed in the present study is provided in Table 2. The average prong tip outlines are compared in Fig 16. Recall that these averages generally represent the results for five C-Rings. The measurements for each individual C-Ring can be found in Ref. [47].

Table 2 shows that the two CF8M sets of experiments resulted in the largest average gap closing among the four steels (i.e., 0.63 mm on average for the side and vertical immersion sets together). As already mentioned, the CF8M experiments also produced the most consistent results, as can be seen in Table 2 by the relatively low standard deviation for these experiments. The average gap closings for the experiments with the three different carbon and low-alloy steels are: 0.32 for the two 1022 sets; 0.41 for the two 4320 sets; and 0.09 for the two 8625 sets. These six sets of experimental results had generally larger standard deviations in the average gap change than the two CF8M sets. The fact that the carbon and low-alloy C-Ring gaps closed less than the CF8M C-Ring gaps must generally be attributed to the phase transformations occurring during heat treatment of these non-austenitic steels [30-31]. The reason for the larger scatter in the carbon and low-alloy steel results is presently unclear (see also the Conclusions section).

Table 2. Summary of average gap openings for all eight sets of experiments

Steel	Immersion Direction	Average Gap Opening, mm	Standard Deviation, mm
CF8M	Side	-0.71	0.16
CF8M	Vertical	-0.55	0.12
1022	Side	-0.33	0.35
1022	Vertical	-0.30	0.26
4320	Side	-0.18	0.29
4320	Vertical	-0.64	0.83
8625	Side	-0.25	0.24
8625	Vertical	0.07	0.21

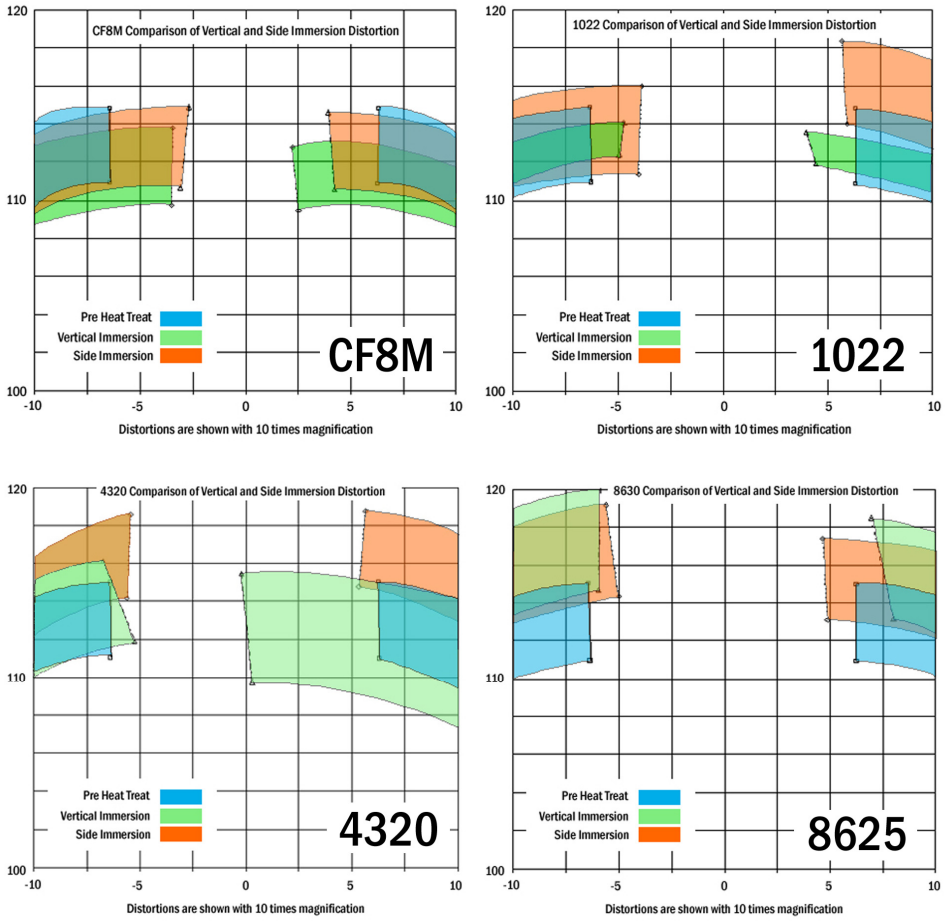

Figure 16. Average prong tip outlines for all eight sets of experiments, shown with 10 times amplification of the deformations

Before discussing the results in Fig. 16 in more detail, it is important to note the large, but physically unrealistic shrinkage or enlargement of some of the prong tips from before to after heat treatment. This is a consequence of large scatter among the measurements for the (generally) five individual C-Rings to which a single post heat treat average prong tip outline corresponds. The prong tip corners sometimes move in opposite directions in the five experiments [47], which can result in the average outline not being similar in shape to the original prong tip.

For the 1022 cast steel C-Rings, the side immersion resulted in significant asymmetry in the distortion, with the right prong tip moving strongly upward (the directions refer to the orientation of the C-Rings as shown in Figs. 16). On the other hand, for the 4320 experiments, the vertical immersion C-Rings show a large amount of asymmetry, with the right prong tip moving strongly to the left. This behavior is not easily explained, since vertical immersion is generally expected to result in symmetric distortions. However, note in Table 2 the large standard deviation in the

gap opening measurements for these experiments. The distortion of the 8625 C-Rings was relatively symmetric for both the vertical and side immersion cases.

Whereas the CF8M C-Ring prong tips moved inward during heat treatment, the carbon and low-alloy steel C-Ring prong tips generally moved outward (away from the C-Ring center). This is particularly apparent in Fig. 16 for the vertical and side immersion 8625 C-Rings. The 8625 experiments also resulted in the smallest gap length changes among the eight sets of experiments, with the 8625 vertical immersion experiments being the only set where, on the average, the gap opened (see Table 2).

Simulations

This section first explains the procedures used to perform the DANTE simulations, which is followed by a detailed presentation of the predicted results for the 1022 vertical immersion experiments. Then, a summary of the simulation results for all carbon and low-alloy steel experiments is provided. The CF8M experiments could not be simulated using DANTE.

Simulation Procedure. DANTE simulation files were created in two steps: first, an input file was written in ABAQUS, and then they were modified slightly for use in the DANTE subroutines. The geometry simulated is shown in Figure 17. The C-Ring was modeled in SolidWorks using the machining dimensions given in Appendix A, but without the support holes, thermocouple holes, and the locating groove. These features were removed in the model, because partitioning and meshing strategies did not resolve the mesh analysis warnings for the original model, regardless of the element size. The final FEA mesh consisted of 4816 nodes that form 3570 eight node brick elements.

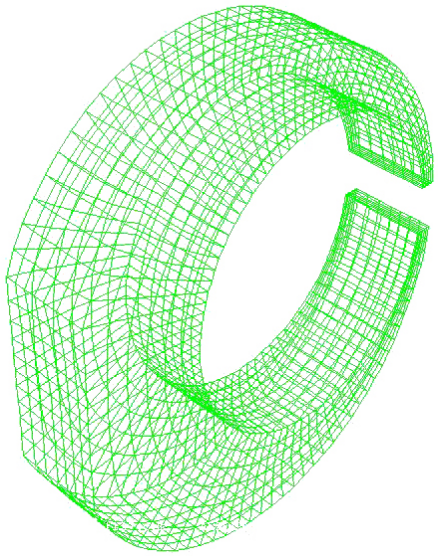

Figure 17. Image of mesh used in the simulations of the 1022 and 4320 cast steel C-Rings

Material properties were then assigned to the part. One hundred "Solution Dependant Variables" (SDV) were included in the material definition. DANTE requires the SDVs to store results for items not normally associated with FEA solvers, such as the phase fractions and hardness. The steps of the heat treatment cycle, interactions on each surface, and film properties (such as heat transfer coefficients) for the process were then input.

The heat treatment simulations included the heat up to 881ºC in the furnace for over 30 minutes, the air transfer of 10 seconds, a quick immersion step of 1 second followed by a quench step for another 6 minutes to the temperature of the water in the quench tank, and then an air cool step to the temperature of the air-conditioned laboratory in which the dimensional measurements were made.

Finally the boundary and initial conditions were applied and a DANTE input file was written. Examples of creating input files for DANTE simulations, along with detailed information regarding the changes that are required to simulate a certain heat treatment process, can be found in Refs. [47, 48]. Post processing was done using ABAQUS CAE.

Results of the 1022 Cast Steel Vertical Immersion Simulation. The predicted deformations for the 1022 vertical immersion simulation, shown with 30 times magnification, are presented after each heat treatment step in Fig. 18. The DANTE simulation predicts that the gap length increases by 0.189 mm, from the initial value of 12.59 mm to the final value of 12.779 mm.

The predicted x-direction gap length is plotted as a function of time in Fig. 19. The figure illustrates the complex nature of the deformations occurring throughout the heat treat cycle. Initially, the non-uniform heating throughout the part results in a "wavy" variation of the gap length. The immediate closing of the gap is principally due to the thermal expansion of the quickly heating prong tips. This closure is then reversed as two phenomena occur simultaneously. First, the continued thermal expansion of the entire ring increases the gap length. Second, the transformation of the prong tips to the denser austenite phase also causes the gap length to increase. The subsequent decrease in the gap length is due to the entire ring converting to austenite. With sufficient time in the furnace, the gap length reaches a constant value. The total gap length increase in the furnace is about 0.1 mm.

The water immersion and quench steps can be seen in Fig. 19 as a sharp spike of nearly 1 mm in magnitude where the gap first opens and then quickly closes again. During quenching, the prong tips respond first and contract until they reach the Ac_3 temperature. This causes the gap to open. The ensuing phase transformations and thermal contractions of the entire ring then cause the gap to close again. Compared to the large spike, the predicted overall change in the gap length during quenching is relatively small (less than 0.1 mm).

The physical processes occurring during heat treatment of the C-Rings are similar for all of the carbon and low-alloy steels and immersion directions [47]. The main difference between the simulations is the magnitude of the gap re-closing during quenching.

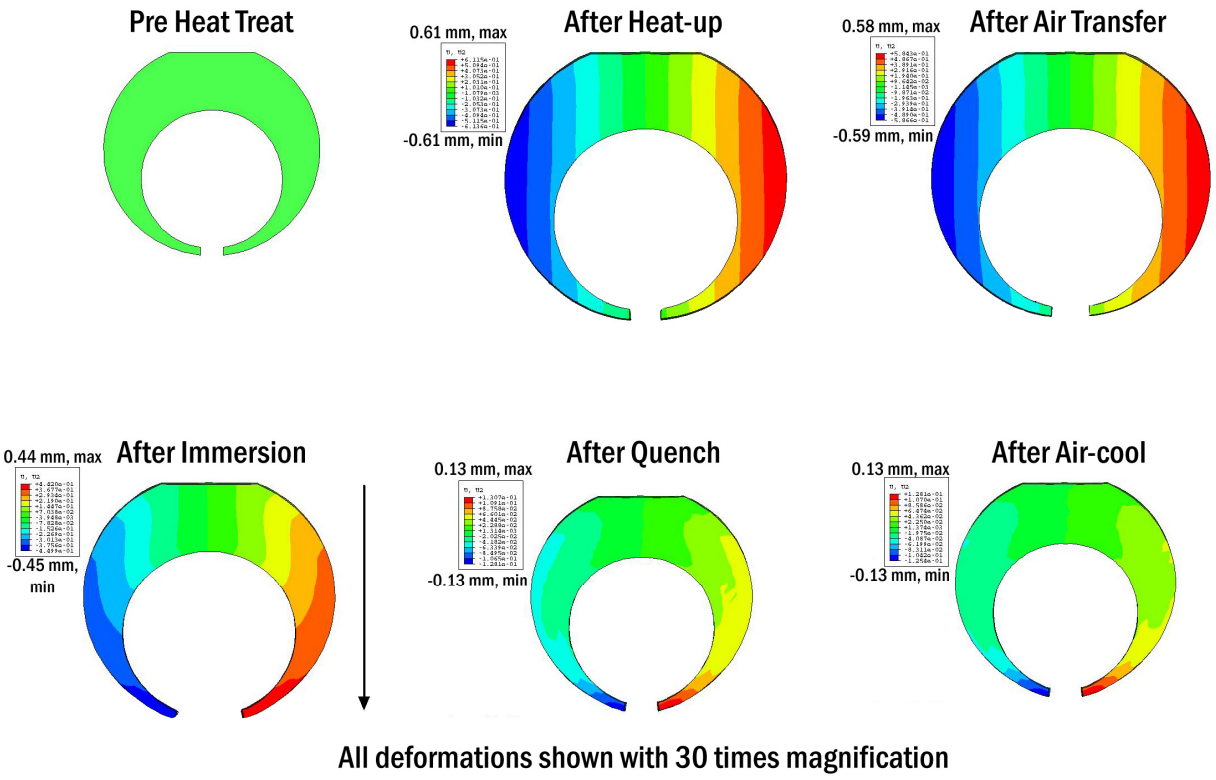

Figure 18. Predicted x-direction deformations during the 1022 cast steel vertical immersion heat treatment cycle

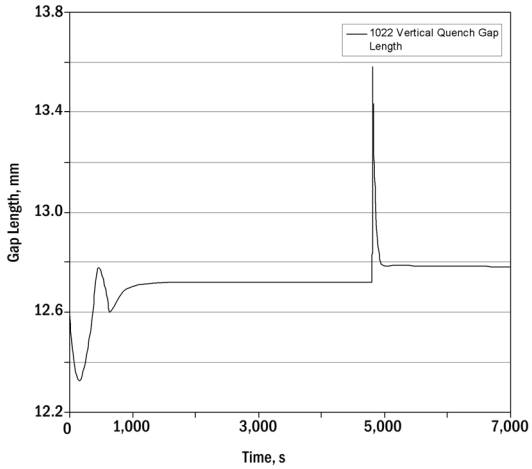

Figure 19. Predicted gap length evolution throughout the heat treatment cycle (1022 vertical immersion simulation)

The final phase fraction distributions from the 1022 vertical immersion water quench simulation are shown in Fig. 20. In the thick section of the C-Ring, a mixture of about 70% pearlite and 30% ferrite is predicted to be present after heat treatment. This can also be seen in Fig. 21, where the predicted phase fractions are plotted as a function of time at the location of the thermocouple hole (which is located in the thick section). Only the prong tips show a significant fraction of martensite (up to about 80%) in the post heat treat condition. Predicted final phase fraction distributions for all other simulations can be found in Ref. [47].

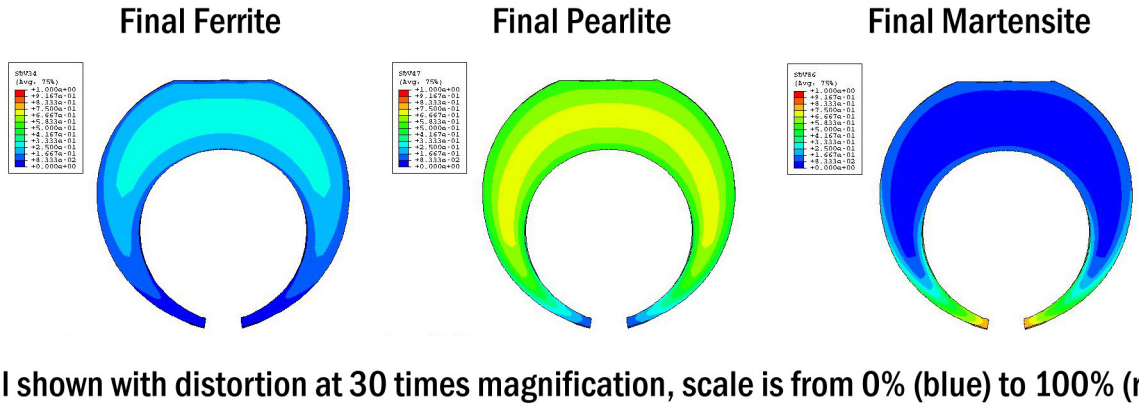

Figure 20. Predicted final phase fraction distributions for 1022 cast steel vertical immersion water quench heat treatment

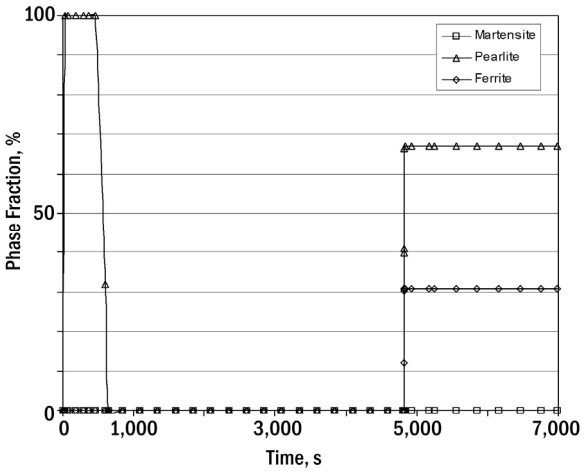

Figure 21. Predicted phase fraction evolution at the location of the thermocouple hole throughout the heat treatment cycle (1022 vertical immersion simulation)

Summary of Simulation Results for All Carbon and Low-Alloy Steels. Five of the six carbon and low-alloy steel heat treatment experiment sets were simulated successfully. The 8625 simulations required that a quarter-geometry with two symmetry planes be used; therefore, no side immersion simulations could be executed. A complete discussion of this problem is given in Ref. [47]. The predicted gap length changes for each of the five successful simulations are provided in the last column of Table 3.

Table 3. Comparison of measured and predicted gap openings

Steel	Immersion Direction	Measured Average Gap Change, mm	Measured Standard Deviation, mm	DANTE Predicted Gap Change, mm
1022	Side	-0.33	0.35	0.160
1022	Vertical	-0.30	0.26	0.189
4320	Side	-0.18	0.29	0.0045
4320	Vertical	-0.64	0.83	0.235
8625	Side	-0.25	0.24	NA
8625	Vertical	0.07	0.21	0.403

In all simulations, the gap is predicted to open upon heat treatment. This is consistent with simulation results previously reported in the literature [31-32]. However, significant differences can be observed in Table 3 in the predicted gap length changes between the various steel grades and immersion directions. For vertical immersion, the predicted gap opening changes from 0.189 mm to 0.235 mm to 0.403 for the 1022, 4320 and 8625 cast steels, respectively. Generally, the gap is predicted to open less for the side immersion cases than for the vertical immersion cases. While the difference is relatively insignificant for the 1022 cast steel, it is nearly 0.2 mm for the 4320 cast steel. Almost no gap length change is predicted for the 4320 side immersion case.

Comparison of Measured and Predicted Gap Length Changes

A comparison of measured and predicted gap length changes due to heat treatment is also provided in Table 3. Generally, the simulations predict a significantly larger increase in the gap length than observed in the experiments. In fact, in most experiments the gap change was negative, while a gap opening is observed in all simulations. On the average, the gap length change is over-predicted by roughly 0.5 mm. However, it should be kept in mind that the experimental results for the carbon and low-alloy steels showed a relatively large scatter, as can be seen from the standard deviations listed in Table 3. For example, for the 4320 cast steel C-Rings the predicted gap length changes are actually within one standard deviation of the measured average gap changes.

The simulations do reflect some of the trends seen in the experimental results. For example, the fact that the predicted gap opening is the largest for the 8625 C-Rings is born out by the experiments in that the measured average gap change for the 8625 vertical immersion C-Rings is

the only one that is positive. The fact that the immersion direction has little effect on the gap length changes for the 1022 C-Rings is seen in both the measured and predicted results. The prediction that the gap length change is near zero for the 4320 side immersion case is also seen in the measurements.

Conclusions

A test part, similar in nature to the Navy C-Ring, was heat treated in a designed experiment to evaluate the commercial heat treatment distortion simulation software DANTE. A total of 40 C-Rings were cast of CF8M, 1022, 4320 and 8625 steel and subsequently machined to the desired pre heat treat dimensions. The heat treatment cycle consisted of heating to 881ºC in a furnace and quenching in an agitated water bath. Two different immersion directions were employed during the quench. The distortions of the C-Ring prong tips due to heat treatment were measured using a CMM. Heat transfer coefficients were determined from temperature measurements performed during the CF8M experiments. The carbon and low-alloy steel heat treat experiments were simulated with DANTE, and measured and predicted C-Ring gap length changes were compared.

While some of trends in the measured C-Ring gap length changes are predicted by the DANTE simulations, a relatively consistent difference of roughly 0.5 mm is observed between the measured and predicted gap changes. In all but one of the experiment sets, closing of the C-Ring gap is observed, while the simulations always predict a gap opening. Some of the discrepancies between the experiments and the simulations may be attributed to the fact that there is a relatively large scatter in the carbon and low-alloy steel C-Ring measurements. However, the consistency in the dimensional measurements for the CF8M C-Rings indicates that the present experimental procedures are accurate and repeatable. Therefore, it is likely that the scatter in the carbon and low-alloy steel results is caused by inconsistencies in the as-cast structure of these C-Rings. Although all C-Rings for a given set of experiments were cast from the same heat, such inconsistencies can still be present due to different porosity and oxide inclusion distributions in the as-cast carbon and low-alloy steel C-Rings. Such differences are presumably not present in the CF8M C-Rings. Hence, it is recommended that the C-Rings used in the present experiments be examined for internal casting discontinuities. Note that previous literature [30, 31] indicates that DANTE predictions generally agree well with measurements made on C-Rings or other part geometries that are machined from stock and are likely to be sound. Metallurgical analysis of the present C-Rings should also be performed, in order to compare measured and predicted phase fraction distributions.

While the lack of agreement between the distortions measured and predicted in the present study may seem discouraging, it should be kept in mind that the final distortions of the C-Rings are all relatively small and the result of much larger deformations during the heat treatment process itself. Therefore, a C-Ring may not be the best geometry to validate heat treatment simulation predictions for steel castings. It is recommended that the DANTE software be evaluated for large productions steel castings that experience significant heat treatment distortions. However, it should be kept in mind that it is difficult to perform accurate and repeatable dimensional measurements on such production castings.

Acknowledgements

This research was funded by the United States Department of Energy as part of the Energy-Saving Melting and Revert Reduction Technology (E-SMARRT) research program under award number DE-FC36-04GO14230. It is also conducted under the auspices of the Steel Founders' Society of America, and through substantial in-kind support, guidance and interest from SFSA member foundries. The authors would like to thank DTC Inc. and MAGMA GmbH for their generous support through donation of software, time and information. Personally, the authors would like to thank Dr. F. Peters of Iowa State University, Mr. Z. Li of DTC Inc., Mr. B. Bryant of Keokuk Steel Castings, Mr. H. Davis and Mr. T. Alias of Sivyer Steel Corp. and Mr. D. Daily of Wollaston Alloys. Mr. J.R. Pratt is thanked for his help with the dimensional measurements. Any findings, opinions, and conclusions or recommendations expressed in this paper are those of the authors and do not necessarily reflect the views of the Department of Energy.

References

1. Ferguson, B. L., Freborg, A. M., Petrus, G., and Callabresi, M. L., *Gear Technology,* November/December 2002, 20-25.
2. Cho, J. R., Kang, W. J., Kim, M. G., Lee, J. H., Lee, Y. S., Bae, W. B., *J. of Mat. Proc. Tech.,* **153-154** (2004) 476-481.
3. Rohde, J., Jeppsson, A., *Scandinavian Journal of Metallurgy,* **29** (2000) 47-62.
4. Hardin, R., Beckermann, C., *SFSA 59th T&O Conference*, Chicago IL, 2005.
5. Ferguson, B. L., Li, Z., Freborg, A. M., *Comp. Mat. Sci.,* **34** (2005) 274-281.
6. Prantil, V. C., Callabresi, M. L., Lathrop, J. F., Ramaswamy, G. S., Lusk, M. T., *Eng. Mat. and Tech. Trans. of the ASME,* **125** (2003) 116-124.
7. Ju., D.Y., Zhang, W.M., Zhang, Y., *Mat. Sci. and Eng. A*, **438-440** (2006) 246-250.
8. Chen, J.R., Tao, Y.Q., Wang, H.G., *J. of Mat. Proc. Tech.,* **63** (1997) 554-558.
9. Inoue, T., Arimoto, K., *Proc. of the First Int. Conf. on Quenching and Control of Distortion,* Chicago IL, 1992.
10. Krauss, G., *Proc. of the First Int. Conf. on Quenching and Control of Distortion,* Chicago IL, 1992.
11. Henriksen, M., Larson, D.B., Van Tyne, C.J., *Proc. of the First Int. Conf. on Quenching and Control of Distortion,* Chicago IL, 1992.
12. Buchmayr, B., Kirkaldy, J.S., *Proc. of the First Int. Conf. on Quenching and Control of Distortion,* Chicago IL, 1992.
13. Clements, T.E., Chuzhoy, L., Shareef, I., *Proc. of the Second Int. Conf. on Quenching and Control of Distortion,* Chicago, IL, 1996.
14. Denis, A., Simon, A., *Proc. of the Second Int. Conf. on Quenching and Control of Distortion,* Chicago, IL, 1996.
15. Chen, X.L., Meekisho, L., *Proc. of the Second Int. Conf. on Quenching and Control of Distortion,* Chicago, IL, 1996.
16. Ju. D.Y., Sahashi, M., Omori, T., Inoue, T., *Proc. of the Second Int. Conf. on Quenching and Control of Distortion,* Chicago, IL, 1996.
17. Ikuta, F., Arimoto, K., Inoue, T., *Proc. of the Second Int. Conf. on Quenching and Control of Distortion,* Chicago, IL, 1996.

18. Oldenburg, M., Bergman, G., Sandberg, L., Jonsson, M., *Proc. of the Second Int. Conf. on Quenching and Control of Distortion,* Chicago, IL, 1996.
19. Baker, A.J., Manhardt, P.D., Orzechowski, J.A., *Proc. of the Second Int. Conf. on Quenching and Control of Distortion,* Chicago, IL, 1996.
20. Gur, C.H., Tekkaya, A.E., Ozturk, T., *Proc. of the Second Int. Conf. on Quenching and Control of Distortion,* Chicago, IL, 1996.
21. Palafox, M.G., Colas, R., *Proc. of the Second Int. Conf. on Quenching and Control of Distortion,* Chicago, IL, 1996.
22. Dowling Jr., W., Shick, D., Pattock, T., Gu, H.Y., Ferguson, B.L., Howes, M., *Proc. of the Second Int. Conf. on Quenching and Control of Distortion,* Chicago, IL, 1996.
23. Shick, et al., *Proc. of the Second Int. Conf. on Quenching and Control of Distortion,* Chicago, IL, 1996.
24. Bammann, D., Prantil, V., Kumar, A., Lathrop, J., Mosher, D., Callabresi, M., et al, *Proc. of the Second Int. Conf. on Quenching and Control of Distortion,* Chicago, IL, 1996.
25. Anderson, C., Goldman, P., Rangaswamy, P., et al, *Proc. of the Second Int. Conf. on Quenching and Control of Distortion,* Chicago, IL, 1996.
26. Wei, S., Zhuang, L., "Prediction of Internal Stresses, Phase Transformations and Research on Numerical Simulation of Quenching," *Proc. of the Fourth Int. Conf. on Quenching and Control of Distortion,* Beijing, 2003.
27. Li, M.V., Totten, G.E., *Proc. of the Fourth Int. Conf. on Quenching and Control of Distortion,* Beijing, 2003.
28. Wei, S., Ke-fu, Y., Chun-cheng, L., Zhuang, L., *Proc. of the Fourth Int. Conf. on Quenching and Control of Distortion,* Beijing, 2003.
29. Deformation Control Technology, Inc., website homepage, http://deformationcontrol.com/, 2006.
30. French, H.J., The Quenching of Steels, American Society for Steel Treating, Cleveland, OH, 1930.
31. Li, Z., Ferguson, B.L., Sun, X., Bauerle, P., Proc*. of the 23rd ASM Heat Treating Society Conference*, Pittsburgh, PA, 2005.
32. Hernandez-Morales, B., Barba-Mendez, O., Ingalss-Cruz, A., Barrera-Godinez, J.A., *Int J. of Mat. and Product Tech.,* **24** (2005) 306-318.
33. Personal correspondence with researchers with experience using CMM for deformation measurements, 2006.
34. Carey, V.P., Liquid-Vapor Phase-Change Phenomena: An Introduction to the Thermophysics of Vaporization and Condensation Processes in Heat Transfer Equipment, Taylor & Francis, 1992.
35. Totten, G.E., Bates, C.E., Clinton, N.A., Handbook of Quenchants and Quenching Technology, ASM International Press, Materials Park, OH, 1993.
36. Kuyucak, S., Newcombe, P., Bruno, P., Grozdanich, R., Looney, G., *SFSA T&O Conference*, Chicago, IL, 2001.
37. Segerberg, S., Bodin, J., *Proc. of the First Int. Conf. on Quenching and Control of Distortion,* Chicago IL, 1992.
38. Bates, C.E., "Evaluating the Effects of Quenching Variables of Hardening Steels, SFSA Technical Paper 95," Carbon and Low-alloy Research Committee, 1982.
39. Beck, J.V., Blackwell, B., St. Clair, C.R. Jr., Inverse Heat Conduction: Ill-Posed Problems, Wiley-Interscience, 1985.

40. Franca, F.H.R., Ezekoye, O.A., Howell, J.R., *Trans. Of ASME*, **123** (2001) 884-891.
41. Vynnycky, M., Ferrari, J., Lior, N., *J. of Heat Transfer*, **125** (2003) 1-10.
42. Zhou, J.W., Mahulikar, S.P., *Experimental Heat Transfer*, **19** (2006) 297-308.
43. Penha, R.N., Canale, L.C.F., Totten, G.E., Sarmiento, G.S., Venture, J.M., *J. of ASTM International*, **3** No. 5, (2006).
44. Sozbir, N., Chang, Y.W., Yao, S.C., *Transaction of the ASME*, **125** (2003) 70-74.
45. Ozenik, M.N., Inverse Heat Transfer: Fundamentals and Applications, Taylor & Francis, 2001.
46. Varkey, V.K., Voight, R.C., *SFSA 55th T&O Conference*, Chicago, IL, 2001.
47. Brooks, B., *The Prediction of Heat Treatment Distortion of Cast Steel C-Rings*, Masters Thesis, The University of Iowa, 2007.
48. Help file from DANTE, Version 3.0.

APPENDIX A

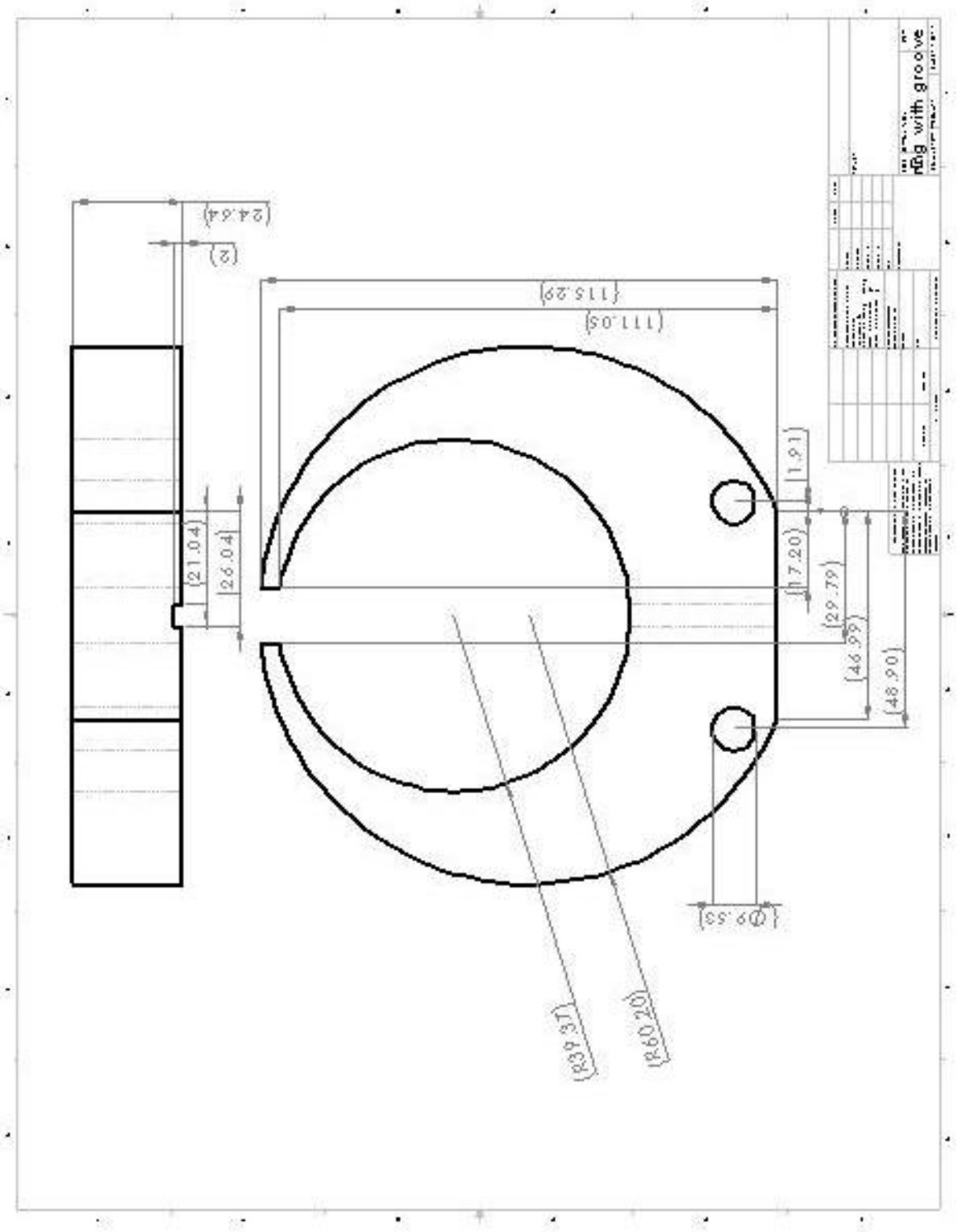
24.64
2
115.29
111.05
1.91
17.20
29.79
46.99
48.90
21.04
26.04
Ø9.53
839.37
860.20
ring with groove